Convective instability in protein crystal growth

D. Lima* and A. De Wit
Service de Chimie-Physique, Centre for Nonlinear Phenomena and Complex Systems, CP 231, Université Libre de Bruxelles, Campus Plaine, 1050 Brussels, Belgium

(Received 9 March 2004; revised manuscript received 2 June 2004; published 17 August 2004)

The conditions for the onset of convection during protein crystalization from a solution are studied theoretically on the basis of diffusion-convection evolution equations for the concentrations coupled to the Navier-Stokes equation describing the flow velocity. We consider that the density of the solution depends on the concentration of two species, namely, a protein and a precipitating agent, a salt. While the protein is crystallized at the crystal/solution interface, the salt is rejected, and these mechanisms are described by means of boundary conditions for the interface. We find the base profiles for both protein and salt concentrations and perform a linear stability analysis of this basic state with regard to buoyancy induced perturbations. This gives information on the critical diameter of capillaries above which convection may be observed, as well as on the influence of the speed of growth V of the crystal interface on the stability of the system. Numerical integration of the model shows good agreement with the predictions of the linear stability analysis.

DOI: 10.1103/PhysRevE.70.021603 PACS number(s): 81.10.Aj, 81.10.Dn, 87.14.Ee, 47.20.Bp

I. INTRODUCTION

In recent years many experiments have been carried out in space to grow protein crystals of improved quality (review in Refs. [1,2]). Growth of protein crystals in microgravity conditions may, ideally, decrease the number of defects in the crystal thanks to the absence of convection in the solution. Such convection arises in the case of crystals growing from solution because of the presence of a depletion zone around the crystals [3]. Indeed, when a crystal grows, it depletes the solution around it as protein is incorporated into the crystal. A density gradient is therefore installed in the depletion zone where the protein concentration changes gradually from its value at the crystal interface up to the bulk concentration. These density gradients may thus cause the onset of convective instability if gravitational acceleration is not perpendicular to the density gradient. Such a buoyancy-driven instability has been observed both experimentally [4] and in numerical simulations of protein crystal growth [5,6]. In crystal growth experiments performed in microgravity motions of the crystals in different directions have been observed [7,8], which could be evidence of convection. It is thus important to be able to predict and avoid the conditions for onset of convection both on Earth and in microgravity conditions. In particular, it is important to have insight into the influence of the peculiarities of the protein at hand as well as of the presence of a precipitating agent such as a salt, for instance, on the buoyancy driven instability. To do so, we perform a linear stability analysis of a two-variable (the protein and a salt) diffusion-convection model of protein crystal growth taking the kinetics of the crystallization into account through boundary conditions at the crystal-solution interface.

Modeling protein crystal growth is a difficult task, as many factors and steps have to be taken into account, such as nucleation, dissolution, growth, etc. However, a simpler approach can be taken which focuses on an already growing crystal and studies the fluid dynamics interplay with the solution/crystal interface [5]. The nucleation process is thus not considered here as we start with a crystal already growing in the reactor. The system is taken as isothermal and since at this stage morphological instabilities are not considered, the interface solution/crystal is flat. To focus on buoyancy induced fluid motions in the solution, we take into account the fact that both protein and salt concentrations contribute to density variations. The protein crystallizes at the interface causing the appearance of a protein depleted zone in the solution in the region close to the solution. The salt, on the other hand, is rejected at the interface leading to a slight increase in the salt concentration close to the crystal. These effects are introduced in our model via boundary conditions at the interface which also take into account the incorporation of protein by the crystal and the flow of protein to its surface. The aim of this paper is to study the convective instability in such a system. In order to do so, we perform a linear stability analysis of the base state of our model with regard to buoyancy induced convection in order to predict regions in the parameter space where convective instability is expected to occur. Results of our stability analysis are then confronted to nonlinear simulations. This gives insight into the influence of parameters such as the kinetic coefficient β (related to the growth speed V of the crystal/solution interface) or the diameter of the capillaries in which crystallization takes place on the onset of convection.

This article is organized as follows. In Sec. II, we set up the model at the basis of our theoretical analysis. We establish its base state in Sec. III. We then perform a linear stability analysis of this base state with regard to convection in Sec. IV and discuss dispersion curves in Sec. V. The results of the linear stability analysis are confronted to nonlinear simulations in Sec. VI before we conclude.

II. THE MODEL

We consider a two-dimensional system consisting of a semi-infinite reactor as shown in Fig. 1. An already growing

*Electronic address: dlima@ulb.ac.be

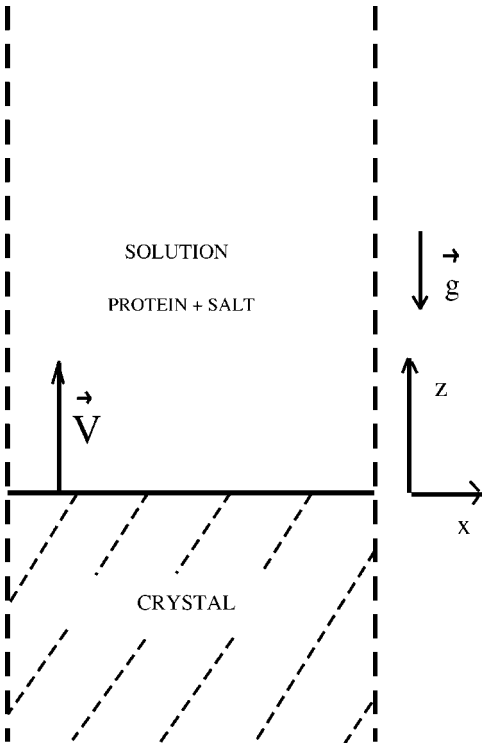

FIG. 1. Sketch of the semi-infinite reactor.

crystal with a flat surface perpendicular to direction $\boldsymbol{z}$ grows upwards with growth velocity V. In a frame of reference moving with velocity V the governing equations are

$$\boldsymbol{\nabla}\cdot\boldsymbol{u}=0, \tag{1}$$

$$\frac{\partial \boldsymbol{u}}{\partial t}+(\boldsymbol{u}\cdot\boldsymbol{\nabla})\boldsymbol{u}-V\frac{\partial \boldsymbol{u}}{\partial z}=-\frac{\boldsymbol{\nabla}p}{\rho_0}+\nu\boldsymbol{\nabla}^2\boldsymbol{u}-\frac{\rho(C_1,C_2)}{\rho_0}g\boldsymbol{k}, \tag{2}$$

$$\frac{\partial C_1}{\partial t}+(\boldsymbol{u}\cdot\boldsymbol{\nabla})C_1-V\frac{\partial C_1}{\partial z}=D_1\boldsymbol{\nabla}^2C_1, \tag{3}$$

$$\frac{\partial C_2}{\partial t}+(\boldsymbol{u}\cdot\boldsymbol{\nabla})C_2-V\frac{\partial C_2}{\partial z}=D_2\boldsymbol{\nabla}^2C_2, \tag{4}$$

$$\rho(C_1,C_2)=\rho_0[1+\beta_1(C_1-C_1^{\infty})+\beta_2(C_2-C_2^{\infty})], \tag{5}$$

where Eq. (1) is the continuity equation, Eq. (2) is Navier-Stokes equation in the Boussinesq approximation giving the evolution of the two-dimensional fluid velocity $\boldsymbol{u}=(u_x,u_z)$. Equations (3) and (4) are the diffusion-convection equations for protein C_1 and salt C_2 concentrations in the solution (expressed here in g/cm^3). C_1^{∞} and C_1^{∞} are the bulk protein and salt concentrations, which remain constant and that we use here as reference concentrations. The density ρ of the solution is supposed to vary linearly with the concentrations. ρ_0 is the density of the bulk solution (i.e., the density when $C_1=C_1^{\infty}$ and $C_2=C_2^{\infty}$) while β_1 and β_2 are the solutal expansion coefficient for protein and salt, respectively. D_1 and D_2 are the protein and salt diffusion coefficients, ν is the kinematic viscosity, and g the gravitational acceleration. This system must be completed by boundary conditions at the interface between the crystal and the solution ($z=0$) and in the bulk ($z=\infty$). We know that the protein is being crystallized and that this process creates a protein depleted zone at the interface [5]. On the other hand, salt is being rejected at the interface. The boundary conditions for the protein concentration at the interface which incorporate the kinetics can be written as [9]

$$D_1\frac{\partial C_1}{\partial z}=\rho(C_1^c-C_1)V, \tag{6}$$

$$D_1\frac{\partial C_1}{\partial z}=\beta(C_1-C_1^{\mathrm{eq}}), \tag{7}$$

where C_1^c is the concentration of the protein in the crystal and $\rho=\rho^c/\rho^s$ is the ratio of the crystal ρ^c and solution ρ^s densities. C_1^{eq} is the equilibrium concentration, i.e., the solubility, while C_1 is here the protein concentration measured at the interface, i.e., $C_1|_{z=0}$. Equation (6) expresses the conservation of mass for the protein in the sense that the normal diffusion flux [left-hand side of Eq. (6)], is proportional to the normal growth rate of the crystal V. Equation (7) accounts for the incorporation of protein by the crystal which depends on β, the kinetic coefficient. β characterizes the rate at which molecules are incorporated at the interface. The interface velocity or crystal growth rate can be found from Eq. (6) and (7) to be equal to

$$V=\frac{\beta(C_1-C_1^{\mathrm{eq}})}{\rho(C_1^c-C_1)}. \tag{8}$$

V may fluctuate locally on the interface, but for the purposes of this work we consider it as constant over the whole interface. For the salt, conservation of mass at the growing face leads to the following boundary condition at the interface:

$$D_2\frac{\partial C_2}{\partial z}=(\kappa-1)C_2V, \tag{9}$$

where κ is the salt segregation coefficient. Salt is being rejected at the interface, therefore $1<\kappa<0$. C_2 here is the salt concentration measured at the interface. This condition allows one to know how much of the salt arriving at the interface [left-hand side of Eq. (9)] is being rejected by it [right-hand side of Eq. (9)].

Other conditions at the interface are that the normal component of the fluid velocity and its derivatives vanish at the interface

$$u_z=0, \tag{10}$$

$$\frac{\partial u_z}{\partial_z}=0, \tag{11}$$

while at infinity in the bulk, we have

$$u_z=0, \tag{12}$$

TABLE I. Values of the constants for lysozyme in water [5].

Symbol		Value
C_1^c	protein concentration in the protein crystal	0.82 g/cm^3
ρ^c	crystal density	1.233 g/cm^3
ρ^s	solution density	1.020 g/cm^3
D_1	protein diffusion coefficient	1.06 10^{-6} cm^2/s
D_2	salt diffusion coefficient	1.47 10^{-5} cm^2/s
ν	kinematic viscosity	1.53 10^{-2} cm^2/s
C_1^{eq}	lysozyme solubility (T=12 °C, pH=4.5, 2.5% NaCl)	0.0031 g/cm^3
ρ	ρ^c/ρ^s	1.21
β_1	solutal expansion coefficient for the protein	0.3 cm^3/g
β_2	solutal expansion coefficient for the salt	0.6 cm^3/g
g_0	gravitational acceleration on Earth	981 cm/s^2
κ	salt segregation coefficient	0.9

$$C_1 = C_1^{\infty}, \tag{13}$$

$$C_2 = C_2^{\infty}. \tag{14}$$

III. THE STEADY-STATE

The system admits a convectionless steady-state solution for which the fluid velocity is $\boldsymbol{u}=\boldsymbol{u}^S=\mathbf{0}$. The superscript S is used to indicate steady state. The concentration fields can be found from Eqs. (3) and (4) along with the conditions at the interface and at infinity. They lead to

$$C_1^S(z) = C_1^{\infty} - \frac{\beta(C_1^{\infty} - C_1^{\mathrm{eq}})}{(\beta + V)} e^{(-V/D_1 z)} \tag{15}$$

and

$$C_2^S(z) = C_2^{\infty} + C_2^{\infty}\frac{(1-\kappa)}{\kappa} e^{[-(V/D_2)z]}. \tag{16}$$

At the interface ($z=0$) we have

$$C_1^S(0) = C_1^{\infty} - \frac{\beta(C_1^{\infty} - C_1^{\mathrm{eq}})}{(\beta + V)}, \tag{17}$$

$$C_2^S(0) = C_2^{\infty} + C_2^{\infty}\frac{(1-\kappa)}{\kappa}. \tag{18}$$

To obtain explicitely the basic profiles, we fix the protein concentration at the interface $C_1^S(0)$ using data from Ref. [5], compute the growth velocity V of the crystal using Eq. (8) and the protein concentration in the bulk using Eq. (17). Then we fix the salt concentration in the bulk and from Eqs. (15) and (16) we find the basic profiles. Typical values for the protein solubility, the salt segregation coefficient and the diffusion coefficients for salt and protein are given for lysozyme in Table I.

The governing equations and the boundary conditions can be rescaled in order to obtain a nondimensional system using as characteristic length $L=D_1/V$ and time $\tau=D_1/V^2$. The new dimensionless variables are hence $\boldsymbol{r}^*=\boldsymbol{r}/L$, $\boldsymbol{u}^*=\boldsymbol{u}/V$, $p^*=(D_1/\mu V^2)p$, $t^*=t/\tau$, and $C_j^*=(C_j-C_j^{\infty})/C_j^{\infty}$, where
$\mu=\rho_0\nu$. The new equations are (after dropping the stars):

$$\boldsymbol{\nabla}\cdot\boldsymbol{u} = 0, \tag{19}$$

$$S_c^{-1}\left[\frac{\partial \boldsymbol{u}}{\partial t} + (\boldsymbol{u}\cdot\boldsymbol{\nabla})\boldsymbol{u} - \frac{\partial \boldsymbol{u}}{\partial z}\right] = -\boldsymbol{\nabla} p + \nabla^2\boldsymbol{u} - R_1 C_1 \boldsymbol{k} - R_2 C_2 \boldsymbol{k}, \tag{20}$$

$$\frac{\partial C_j}{\partial t} + (\boldsymbol{u}\cdot\boldsymbol{\nabla})C_j - \frac{\partial C_j}{\partial z} = \frac{D_j}{D_1}\boldsymbol{\nabla}^2 C_j, \tag{21}$$

where $j=1,2$ for protein and salt, respectively. $S_c=\nu/D_1$ is the Schmidt number and

$$R_1 = \frac{L^3\beta_1 g C_1^{\infty}}{\nu D_1}, \tag{22}$$

$$R_2 = \frac{L^3\beta_2 g C_2^{\infty}}{\nu D_1}, \tag{23}$$

are the Rayleigh numbers. At the interface, the boundary conditions in dimensionless form become

$$\frac{\partial C_1}{\partial z} = \frac{\beta}{V}\left(C_1 + 1 - \frac{C_1^{\mathrm{eq}}}{C_1^{\infty}}\right), \tag{24}$$

$$\frac{\partial C_2}{\partial z} = \frac{D_1}{D_2}(\kappa - 1)(C_2 + 1), \tag{25}$$

$$u_z = 0, \tag{26}$$

$$\frac{\partial u_z}{\partial z} = 0, \tag{27}$$

and at infinity

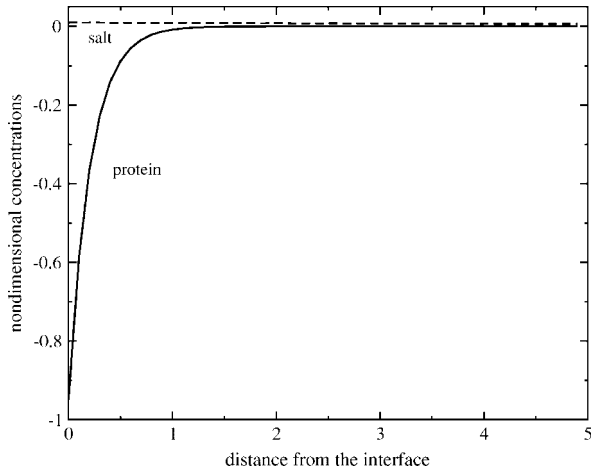

FIG. 2. Profiles of initial nondimensional concentrations for $\beta = 1.0 \times 10^{-4}$ cm/s [Eqs. (31) and (32)].

$$u_z = 0, \tag{28}$$

$$C_1^{\infty} = C_2^{\infty} = 0. \tag{29}$$

The pressure dependence in the Navier-Stokes equation can be eliminated by taking twice the curl of Eq. (20) which leads to

$$S_c^{-1}\left[\frac{\partial \nabla^2 \boldsymbol{u}}{\partial t} - \boldsymbol{\nabla}[\boldsymbol{\nabla}\cdot(\boldsymbol{u}\cdot\boldsymbol{\nabla})\boldsymbol{u}] + \boldsymbol{\nabla}^2(\boldsymbol{u}\cdot\boldsymbol{\nabla})\boldsymbol{u} - \frac{\partial \boldsymbol{\nabla}^2 \boldsymbol{u}}{\partial z}\right] = \boldsymbol{\nabla}^4 \boldsymbol{u} - R_1 \frac{\partial^2 C_1}{\partial x^2} - R_2 \frac{\partial^2 C_2}{\partial x^2}. \tag{30}$$

The nondimensional form of the steady-state solution is given by

$$C_1^S(z) = -\frac{\beta(C_1^{\infty} - C_1^{\mathrm{eq}})}{C_1^{\infty}(\beta + V)} e^{(-z)} \tag{31}$$

and

$$C_2^S(z) = \frac{(1-\kappa)}{\kappa} e^{[-(D_1/D_2)z]}. \tag{32}$$

IV. LINEAR STABILITY ANALYSIS

The typical profiles of the nondimensional concentrations are shown in Fig. 2. The protein profile shows the protein depletion close to the interface, whereas the salt profile is characterized by a higher salt concentration close to the interface due to rejection of salt by the growing face.

Let us now analyze the stability of these base state profiles with regard to buoyantly induced convection. In order to do so, we write the velocity and concentrations as a superposition of the steady-state solution and perturbations

$$(u_x, u_z) = \boldsymbol{u}^S + \epsilon(U, W), \tag{33}$$

$$C_1 = C_1^S + \epsilon\Gamma_1, \tag{34}$$

$$C_2 = C_2^S + \epsilon\Gamma_2. \tag{35}$$

These equations are substituted into Eqs. (21) and (30), as well as into the rescaled boundary conditions. The resulting equations are linearized in ϵ. This leads to the following system of equations for the perturbations:

$$\left(\frac{\partial^2}{\partial z^2} + \frac{\partial^2}{\partial x^2} + \frac{\partial}{\partial z} - \frac{\partial}{\partial t}\right)\Gamma_1 = -C_1^S(z)W, \tag{36}$$

$$\left(\frac{D_2}{D_1}\frac{\partial^2}{\partial z^2} + \frac{D_2}{D_1}\frac{\partial^2}{\partial x^2} + \frac{\partial}{\partial z} - \frac{\partial}{\partial t}\right)\Gamma_2 = -\frac{D_1}{D_2}C_2^S(z)W, \tag{37}$$

$$\left(\frac{\partial^2}{\partial z^2} + \frac{\partial^2}{\partial x^2}\right)\left(\frac{\partial^2}{\partial z^2} + \frac{\partial^2}{\partial x^2} + S_c^{-1}\frac{\partial}{\partial z} - S_c^{-1}\frac{\partial}{\partial t}\right)W = R_1\frac{\partial^2 \Gamma_1}{\partial x^2} + R_2\frac{\partial^2 \Gamma_2}{\partial x^2}. \tag{38}$$

At the interface

$$W = \frac{dW}{dz} = 0, \tag{39}$$

$$\frac{\partial \Gamma_1}{\partial z} - \frac{\beta}{V}\Gamma_1 = 0, \tag{40}$$

$$\frac{\partial \Gamma_2}{\partial z} + \frac{D_1}{D_2}(1-\kappa)\Gamma_2 = 0, \tag{41}$$

while at infinity

$$W = 0, \quad \Gamma_1 = 0, \quad \Gamma_2 = 0. \tag{42}$$

We then express W, Γ_1, and Γ_2 as normal modes

$$W = \Phi(z)e^{-ikx}e^{\sigma t}, \tag{43}$$

$$\Gamma_1 = \Psi_1(z)e^{-ikx}e^{\sigma t}, \tag{44}$$

$$\Gamma_2 = \Psi_2(z)e^{-ikx}e^{\sigma t}, \tag{45}$$

where k is the wave number of the transverse perturbation and σ its growth rate. Substituting these normal modes in the equations for the perturbations, we find σ as the solution of an eigenvalue problem given by

$$\left(\frac{d^2}{dz^2} + \frac{d}{dz} - k^2\right)\Psi_1 + C_1^S(z)\Phi = \sigma\Psi_1, \tag{46}$$

$$\left(\frac{D_2}{D_1}\frac{d^2}{dz^2} + \frac{d}{dz} - \frac{D_2}{D_1}k^2\right)\Psi_2 + \frac{D_1}{D_2}C_2^S(z)\Phi = \sigma\Psi_2, \tag{47}$$

$$k^2R_1\Psi_1 + k^2R_2\Psi_2 + \left(\frac{d^2}{dz^2} - k^2\right)\left(\frac{d^2}{dz^2} + S_c^{-1}\frac{d}{dz} - k^2\right)\Phi = \sigma S_c^{-1}\left(\frac{d^2}{dz^2} - k^2\right)\Phi, \tag{48}$$

and the boundary conditions at the interface

$$\Phi = \frac{d\Phi}{dz} = 0, \tag{49}$$

$$\frac{\partial \Psi_1}{\partial z} - \frac{\beta}{V}\Psi_1 = 0, \tag{50}$$

$$\frac{\partial \Psi_2}{\partial z} + \frac{D_1}{D_2}(1-\kappa)\Psi_2 = 0, \tag{51}$$

while at infinity

$$\Phi = 0, \quad \Psi_1 = 0, \quad \Psi_2 = 0. \tag{52}$$

Equations (46)–(48) can be written as

$$L\begin{bmatrix}\Psi_1\\ \Psi_2\\ \Phi\end{bmatrix} = \sigma\begin{bmatrix}1 & 0 & 0\\ 0 & 1 & 0\\ 0 & 0 & H\end{bmatrix}\begin{bmatrix}\Psi_1\\ \Psi_2\\ \Phi\end{bmatrix}, \tag{53}$$

where

$$H = S_c^{-1}\left(\frac{d^2}{dz^2} - k^2\right), \tag{54}$$

and the elements of the matrix/differential operator L are given by

$$L_{11} = \frac{d^2}{dz^2} + \frac{d}{dz} - k^2, \tag{55}$$

$$L_{13} = \frac{-\beta(C_1^{\infty} - C_1^{\mathrm{eq}})}{C_1^{\infty}(\beta + V)}e^{(-z)} = C_1^S(z), \tag{56}$$

$$L_{22} = \frac{D_2}{D_1}\frac{d^2}{dz^2} + \frac{d}{dz} - \frac{D_2}{D_1}k^2, \tag{57}$$

$$L_{23} = \frac{D_1}{D_2}\frac{(1-\kappa)}{\kappa}e^{(-D_1/D_2 z)} = \frac{D_1}{D_2}C_2^S(z), \tag{58}$$

$$L_{31} = k^2 R_1, \tag{59}$$

$$L_{32} = k^2 R_2, \tag{60}$$

$$L_{33} = \left(\frac{d^2}{dz^2} - k^2\right)\left(\frac{d^2}{dz^2} + S_c^{-1}\frac{d}{dz} - k^2\right), \tag{61}$$

and $L_{12}=L_{21}=0$.

V. DISPERSION RELATIONS

The eigenvalue problem Eq. (53) is solved numerically by means of a second-order central finite-differencing scheme to approximate L and H with their discrete analogs $\mathcal{L}$ and $\mathcal{H}$, respectively. We are then left with a generalized eigenvalue problem. However, multiplying the last equation of the discrete version of Eq. (53) by $\mathcal{H}^{-1}$ we obtain a simple eigenvalue problem. More specifically, if $\mathcal{A}_1$, $\mathcal{A}_2$, and $\mathcal{A}_3$ are the discrete representations of Ψ_1, Ψ_2, and Φ, respectively, the matrix eigenvalue problem has the form $M\mathcal{A}=\sigma\mathcal{A}$, i. e.:

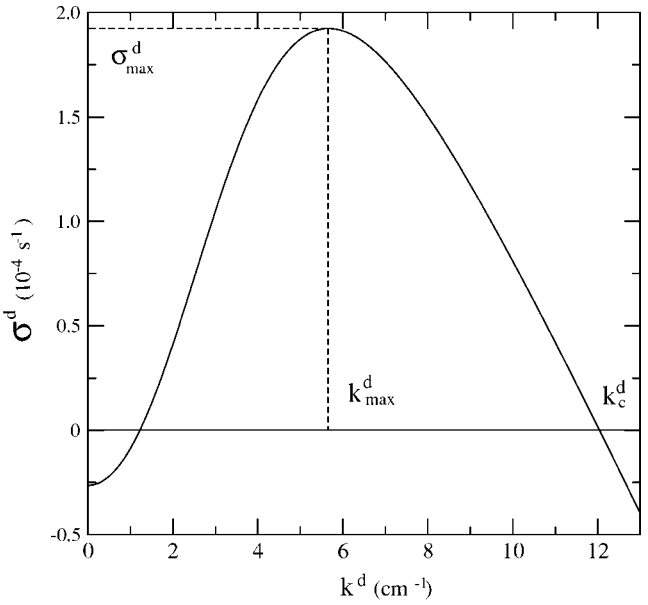

FIG. 3. Dimensional dispersion relation for $\beta=1.3\ 10^{-4}$ cm/s and $g=10^{-6}\ g_0$.

$$\begin{bmatrix}\mathcal{L}_{11} & 0 & \mathcal{L}_{13}\\ 0 & \mathcal{L}_{22} & \mathcal{L}_{23}\\ \mathcal{H}^{-1}\mathcal{L}_{31} & \mathcal{H}^{-1}\mathcal{L}_{32} & \mathcal{H}^{-1}\mathcal{L}_{33}\end{bmatrix}\begin{bmatrix}\mathcal{A}_1\\ \mathcal{A}_2\\ \mathcal{A}_3\end{bmatrix} = \sigma\begin{bmatrix}\mathcal{A}_1\\ \mathcal{A}_2\\ \mathcal{A}_3\end{bmatrix}. \tag{62}$$

The complicated differential eigenvalue problem is so replaced by a much simpler matrix eigenvalue problem. We obtain the eigenvalues and eigenvectors of M using the DGEEVX solver of the LAPACK package. We have calculated σ for the parameters of Table I both for g_0, as well as for microgravity ($10^{-6}\ g_0$). Once the base state profiles are calculated they are inserted into the eigenvalue problem and the spectrum of eigenvalues is calculated as a function of the wave number k. We then come back to dimensional variables and plot the dimensional dispersion curve $\sigma^d=f(k^d)$, where $\sigma^d=\sigma/\tau$ and $k^d=k/L$. A typical dispersion curve plotting the largest eigenvalue of the spectrum $\sigma^d=\sigma^d(k^d)$ is shown in Fig. 3 for microgravity conditions. There is a band of unstable modes for which $\sigma^d>0$. The most unstable wave number is k^d_{max}, corresponding to the mode with largest positive growth rate σ^d_{max}. Convection will appear on a time scale $T=2\pi/\sigma^d_{\mathrm{max}}$ giving a pattern with initial wavelength $\lambda=2\pi/k^d_{\mathrm{max}}$. The critical wave number k^d_c above which all modes are stable ($\sigma^d<0$) provides information on the dimensional critical radius d_c of the system below which no convection will set in:

$$d_c = \frac{2\pi}{k_c^d}. \tag{63}$$

Thus, even if a convective instability is expected to occur, the instability will not be observed if the reactor is not wide enough to allow the formation of at least one convection roll. For proteins growing in capillaries of diameter d, typically, if $d<d_c$ convection will not be observed.

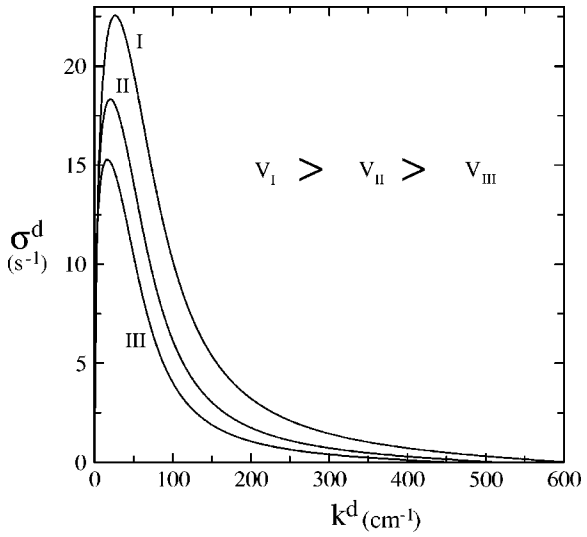

FIG. 4. Dimensional dispersion relation for $g=g_0$ and different kinetic coefficients (and hence different growth velocities V), where $\beta_I > \beta_{II} > \beta_{III}$ ($\beta_I = 1.0\times10^{-4}$ cm/s, $\beta_{II} = 5\times10^{-5}$ cm/s, and $\beta_{III} = 3\times10^{-5}$ cm/s).

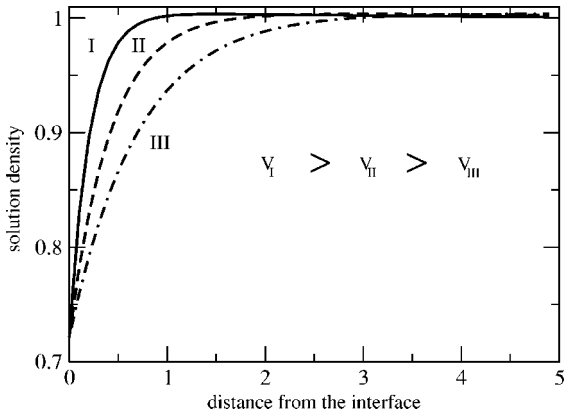

FIG. 5. Dimensionless density profiles for different growth velocities. The values of β are the same as in Fig. 4 where $\beta_I > \beta_{II} > \beta_{III}$ ($\beta_I = 1.0\times10^{-4}$cm/s, $\beta_{II} = 5\times10^{-5}$cm/s, and $\beta_{III} = 3\times10^{-5}$cm/s).

As an example, in microgravity conditions and for parameter values typical of lysozyme (see Table I), we find $d_c \approx 30$ mm for $\beta \approx 10^{-8}$ cm/s, which leads to the conclusion that even though the system is unstable, convection rolls would only be observed in reactors with a width greater than this d_c. This is an indication of how unlikely it is to observe buoyancy-driven convection during growth of lysozyme crystals in microgravity, since these crystals themselves have a width of the order of the millimeter [1]. On earth, for the same parameters, we find $d_c \approx 1$ mm for $\beta \approx 10^{-8}$ cm/s, thus convection is then observable in much thinner reactors, and for realistic crystal sizes.

Let us now analyze how the kinetic coefficient β (typical to each protein) can affect the stability of the system with regard to convection. Figure 4 shows the dispersion relation for different values of β on earth. First of all, the range of unstable wave numbers is much larger than that in microgravity conditions, which is normal. For lysozyme, the corresponding critical diameter d_c below which no convection would set in is $d_c \approx 0.1$ mm for $\beta_1 = 10^{-4}$ cm/s. This clearly shows how unavoidable convection is on Earth.

Dispersion curves give thus an interesting understanding of the influence of the nature of protein (via their kinetic coefficient β) on convection. Increasing β leads to an increase in the growth velocity V of the crystal and to a larger band of unstable modes. As expected a larger growth velocity V leads to a more unstable regime, since faster growth implies more rapid incorporation of proteins into the crystal and hence a given density difference between the crystal surface and the bulk operating on a smaller distance. As Fig. 5 shows, a larger growth velocity implies therefore a greater density gradient, which enhances the strength of the convective instability [9]. In the current system, it is oberved that indeed, when the kinetic coefficient is decreased the system is more stable. The instability threshold depends thus strongly on the kinetic coefficient. We note also that the presence of the salt does not alter the dispersion relation significantly, in agreement with Ref. [5]. This can be explained by the small influence of the salt concentration on the density profile, since the gradient of the salt concentration is much smaller than that for the protein concentration (see Fig. 2) while their solutal expansion coefficient is of the same order.

VI. NONLINEAR DYNAMICS

We have next numerically integrated the Navier-Stokes and diffusion-convection equations for salt and protein. Our code uses a finite-difference method and uniform mesh for the discretization of the system. The new protein and salt concentrations are calculated at each time step, as well as a tentative velocity field that is calculated neglecting the pressure gradient. The pressure field is then calculated from a Poisson equation by means of a successive over relaxation (SOR) method. Then the velocity is updated taking into account the pressure contribution. The numerical results presented here are for the parameters in Table I and g_0. The initial conditions are the convectionless steady state. To check the accuracy of the code, we have tested that it reproduces the results of Lin *et al.* [5]. We have then integrated the nonlinear equations for a quite large system to compare the spontaneous wavelength of the instability appearing in the nonlinear simulations with the one predicted by the linear stability analysis. We take therefore a system of size 2.8 cm large and 0.9 cm height with no-slip and no-flux boundary conditions for the velocity and the concentration fields, respectively, at the lateral sides of the reactor. Conditions (24)–(27) are used at the lower boundary representing the crystal surface while conditions (28) and (29) are applied at the upper boundary. Figure 6 shows the stream function isolines in such a geometry for $\beta = 5\ 10^{-5}$ cm/s for which the linear stability analysis of Fig. 4 predicts that the wavelength of the convective pattern to appear at onset is equal to $\lambda_{max} = 2\pi/k^d_{max} \sim 0.30$ cm. Figure 6 shows that roughly 20 rolls (10 wavelengths) appear in the length of 2.8 cm which gives a wavelength of the convection pattern of the order of 0.28 cm in quite good agreement with the linear stability analysis.

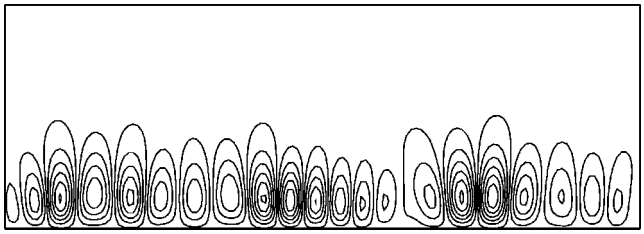

FIG. 6. Stream function isolines for $\beta=5\times10^{-5}$ cm/s (label II on Figs. 4 and 5), length of 2.8 cm and height of 0.9 cm.

The same simulation done for $\beta=1.0\ 10^{-4}$ cm/s provides a convection pattern of wavelength equal to 0.21 cm. This result of a nonlinear simulation is again in good agreement with the predictions given by the dispersion curve of Fig. 4 and, in addition, confirms that increasing β leads to smaller wavelengths (i.e., larger most unstable wave number) and thus to destabilization of the system with regard to convection.

The above simulations were made in a quite large reactor to minimize the effect of lateral boundaries and verify the adequacy with the linear stability analysis. In reality, it is, however, unlikely to find crystals that can span such large systems. Such a situation can only be realized in thin capillaries of diameter of the size of realistic values of crystals say 0.5 cm. On Fig. 7 (top) we show distorted convective rolls for a system with a moderate width that does not match a multiple of the natural wavelength of the instability. The convective rolls are more regular when the width is closer to a multiple of the natural wavelength [Fig. 7 (bottom)]. Nonlinear simulations confirm that systems of width smaller than the critical value of the diameter computed by the linear stability analysis feature a stable situation and no convection.

VII. CONCLUSIONS

We have performed a linear stability analysis of the basic protein and salt profiles during protein crystallization in a two-dimensional semi-infinite reactor. This allows us to predict a critical width of the reactor above which convective instability may be observed. The linear stability analysis allows us also to investigate the importance of different parameters of our model. In particular, we have found that increasing the value of the kinetic coefficient leads to systems that are more unstable.

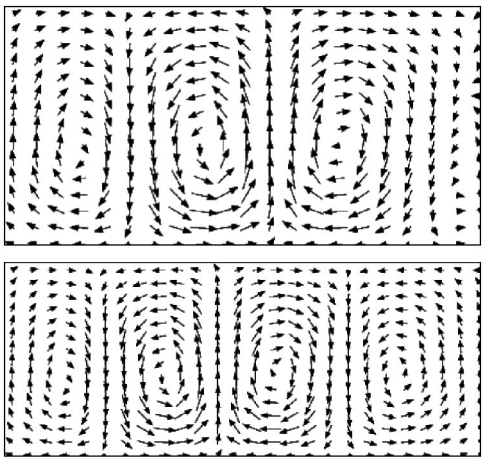

FIG. 7. Convective rolls for $\beta=5\times10^{-5}$ cm/s (label II on Figs. 4 and 5) and for reactors with a height of 0.3 cm and width equal to 0.45 cm (top) and 0.55 cm $\approx 2\lambda_{max}$ (bottom).

The numerical integration of the Navier-Stokes and diffusion-convection equations show good agreement with our predictions. This is an evidence that even though our calculations were carried out for a semi-infinite system, our predictions also remain valid for reactors the size of which are of the order of the wavelength of the convection roll. Work is in progress to take into account crystals with other geometries.

ACKNOWLEDGMENTS

We wish to thank P. Borckmans, L. Carotenuto, I. Zegers, and S. Kalliadasis for fruitful discussions and Prodex (Belgium) for financial support. A.D. is Research Associate of the FNRS (Belgium).

[1] A. Monaco and F. Rosenberger, J. Cryst. Growth **183**, 465 (1993).
[2] S. R. Coriell, A. A. Chernov, B. T. Murray, and G. B. McFadden, J. Cryst. Growth **183**, 669 (1998).
[3] Z. Kam, H. B. Shore, and G. Feher, J. Mol. Biol. **123**, 539 (1978).
[4] M. Pusey, W. Witherow, and R. Naumann, J. Cryst. Growth **90**, 105 (1988).
[5] H. Lin, F. Rosenberger, J. I. D. Alexander, and A. Nadarajah, J. Cryst. Growth **151**, 153 (1995).
[6] M. Lappa, Phys. Fluids **15**, 1046 (2003).
[7] L. Carotenuto, R. Berisio, C. Piccolo, L. Vitagliano, and A. Zagari, J. Cryst. Growth **232**, 481 (2001), and references therein.
[8] F. Otálora, M. L. Novella, J. A. Gavira, B. R. Thomas, and J. M. García Ruiz, Acta Crystallogr., Sect. D: Biol. Crystallogr. **57**, 412 (2001).
[9] C. P. Lee and A. A. Chernov, J. Cryst. Growth **240**, 531 (2002).